Atmosphere **2014**, *5*, 211-229; doi:10.3390/atmos5020211

OPEN ACCESS

atmosphere

ISSN 2073-4433

www.mdpi.com/journal/atmosphere

Article

Analysis and Application of the Relationship between Cumulonimbus (Cb) Cloud Features and Precipitation Based on FY-2C Image

Yu Liu [1], Du-Gang Xi [2,3], Zhao-Liang Li [4,5,*] and Chun-Xiang Shi [6]

[1] Institute of Geographic Sciences and Natural Resources Research, Chinese Academy of Sciences, Beijing 100101, China; E-Mail: liuyu950@126.com

[2] Institute of Geospatial Information, Information Engineering University, Zhengzhou 450001, China

[3] Naval Institute of Hydrographic Surveying and Charting, Tianjin 300061, China; E-Mail: chiduganggis@163.com

[4] Key Laboratory of Agri-Informatics, Ministry of Agriculture / Institute of Agricultural Resources and Regional Planning, Chinese Academy of Agricultural Sciences, Beijing 100081, China

[5] ICube, UdS, CNRS, 300 Bld Sebastien Brant, BP10413, 67412 Illkirch, France

[6] National Meteorological Information Center, China Meteorological Administration, Beijing 100081, China; E-Mail: shicx@cma.gov.cn

* Author to whom correspondence should be addressed; E-Mail: lizl@igsnrr.ac.cn; Tel.: +86-10-6488-9277; Fax: +86-10-6488-9277.

Received: 29 December 2013; in revised form: 25 March 2014 / Accepted: 28 March 2014 / Published: 14 April 2014

Abstract: Although cumulonimbus (Cb) clouds are the main source of precipitation in south China, the relationship between Cb cloud characteristics and precipitation remains unclear. Accordingly, the primary objective of this study was to thoroughly analyze the relationship between Cb cloud features and precipitation both at the pixel and cloud patch scale, and then to apply it in precipitation estimation in the Huaihe River Basin using China's first operational geostationary meteorological satellite, FengYun-2C (FY-2C), and the hourly precipitation data of 286 gauges from 2007. First, 31 Cb parameters (14 parameters of three pixel features and 17 parameters of four cloud patch features) were extracted based on a Cb tracking method using an artificial neural network (ANN) cloud classification as a pre-processing procedure to identify homogeneous Cb patches. Then, the relationship between Cb cloud properties and precipitation was analyzed and applied in a look-up table algorithm to estimate precipitation. The results were as follows: (1) Precipitation increases first and then declines with increasing values for cold cloud and time evolution parameters,

and heavy precipitation may occur not only near the convective center, but also on the front of the Cb clouds on the pixel scale. (2) As for the cloud patch scale, precipitation is typically associated with cold cloud and rough cloud surfaces, whereas the coldest and roughest cloud surfaces do not correspond to the strongest rain. Moreover, rainfall has no obvious relationship with the cloud motion features and varies significantly over different life stages. The involvement of mergers and splits of minor Cb patches is crucial for precipitation processes. (3) The correlation coefficients of the estimated rain rate and gauge rain can reach 0.62 in the cross-validation period and 0.51 in the testing period, which indicates the feasibility of the further application of the relationship in precipitation estimation.

Keywords: FY-2C; cumulonimbus; cloud features; precipitation; Huaihe River Basin

1. Introduction

Cumulonimbus (Cb) clouds, which are intense convective clouds, are often associated with heavy precipitation in the tropics and at the mid-latitudes. Determining the statistical relationship between precipitation and Cb clouds is essential for improving the rainfall estimation algorithms from satellite imagery.

Based on the spatial scales from which cloud features are computed, the analysis of the relationship between cloud features and precipitation can be classified into three categories: pixel-based, window-based and patch-based [1].

A wide variety of studies have been performed to detect the relationship between cloud features and rainfall at the pixel scale. For example, Kurino [2] analyzed the relationship between precipitation and the top brightness temperature (TB) of three infrared (IR) channels of the Geostationary Meteorological Satellite (GMS-5) (IR 11 μm TB (TB_{11}), IR TB difference between 11 μm and 12 μm (TB_{11-12}), and IR TB difference between 11 μm and 6.7 μm ($TB_{11-6.7}$)). Lu and Wu [3] analyzed the precipitation characteristics considering cloud top temperature, temperature gradients and the occurrence of overshooting cloud tops. Those investigations demonstrated that rain usually increases progressively as the cloud-top temperature decreases [4]. However, some studies shows that cold cloud TB does not necessarily imply precipitation due to the existence of cold cloud tops [1,5]. The relationship between cloud characteristics and their generated precipitation remains unclear and needs further detailed analysis at the pixel scale [6–8].

With the introduction of cloud tracking methods, some studies have been performed to identify the impact of cloud development and moving characteristics from the window scale. For example, Griffith *et al.* [6,9] analyzed the rainfall characteristics based on the lifecycle characteristics of clouds. Laurent *et al.* [10] and Mathon *et al.* [11] found that cloud life duration and propagation speed are positively related to the induced precipitation. Goyens *et al.* [12] analyzed the relationship between five cloud parameters (the average propagation speed (Vav), the cloud area at maximum extent (Amax), the life duration (LD), the minimum in BT when averaged over the very cold convective core (BTmin), the time during which the system shows a very cold convective core (LDcc)) and three precipitation variables (3-hourly precipitation averaged over the 10 most rainy pixels (Pmax), averaged over entire

cloud cover (Pav), summed over entire cloud cover (Ptot)) in the Sahel based on tracking mesoscale convective systems (MCSs). Vondou *et al.* [13] investigated the lifecycles of cumulus clouds with cloud-resolving model simulations and found a considerable increase across the composite lifecycles. Almost all those studies have targeted mesoscale convective systems (MCSs) [14], which are ensembles of strong convective cells accompanied by a stratiform region. Somewhat no attention has been devoted to the behavior of individual severe convective activity, such as that of Cb clouds, which typically represents the main source of precipitation. However, the Cb clouds were hard to describe by the traditional window-based methods, due to their irregular and changing shape.

The precipitation characteristics of cloud patches have also been analyzed by some studies. For example, Negri *et al.* [7,8] found that some cloud parameters, such as area, mean cloud temperature and mean visible brightness, are highly correlated to the rainfall volume. Xu *et al.* [1] identified and removed no-rain cold clouds by analyzing the rain probability associated with seven cloud patch features. Most of the studies mainly focus on the cloud static-spatial characteristic, such as the coldness features, geometric features and cloud texture/structure. Temporal characteristics, such as cloud dynamic features, do not appear to have been adequately analyzed. In addition, except for the Cb-TRAM (Cumulonim Bus Tracking And Monitoring) [15], there is no study that has been performed to extract the Cb patch. Thus, no studies analyze the statistical relationship between precipitation and the features of the Cb patch, not to mention its dynamic characteristics. The reason lies in that the determination of Cb cloud patches is a challenging issue in remote sensing sequences, for they are deformable in nature. In addition, it has been observed that Cb cloud patches commonly evolve through a sequence of pulse-like events and are subject to splits and mergers during their lifecycles, which may complicate the tracking of Cb clouds, because the identification criteria that distinguish individual Cb patches are difficult to determine [16–18].

Accordingly, this study aims to thoroughly investigate the statistical precipitation properties of Cb at both the pixel scale and the cloud patch scale and then apply it in a precipitation estimation method, based on a Cb cloud-tracking technique that we first presented with China's first operational geostationary meteorological satellite, FengYun-2C (FY-2C).

The structure of this paper is as follows. The study area and methodology are introduced in Section 2. The statistical precipitation properties of the Cb are analyzed and applied in precipitation estimations in Section 3. The conclusions are provided in Section 4.

2. Study Area and Methodology

2.1. Study Area

The Huaihe River Basin (HRB) (30°55′N~36°36′N and 111°55′E~121°25′E) is located in eastern China, where floods and serious disasters commonly occur. The HRB is the seventh largest river basin in China, with a drainage area of 270,000 km^2 and a population of 165 million. Its annual precipitation is 888 mm, and the majority is generated by Cb clouds [19,20].

2.2. Data

The analysis was performed using 3 FY-2C hourly infrared images (IR1, 10.3–11.3 μm; IR2, 11.5–12.5 μm and water vapour (WV) 6.3–7.6 μm) with a spatial resolution of 5 km at the satellite

bottom point, and the 286 gauge precipitation data provided by the Chinese Meteorological Agency (CMA). The period of interest extended from 1 June to 30 October 2007, when the second largest basin-wide flood since 1954 occurred.

In addition, to clarify the behavior of the application of the relationship between Cb cloud features and precipitation, data from May 2007 and July 2008, were also used.

2.3. Methodology

Although numerous studies exist in the literature on Cb studies in the HRB [19–21], most are local-scale and only treat individual events based on *in situ* meteorological data. There has been no study based on geostationary satellite data for Cb in the HRB, and the relationship between Cb characteristics and their generated precipitation remains unclear. Accordingly, the primary objective of this research is to thoroughly analyze the relationship between Cb cloud features and precipitation both at the pixel and cloud patch scales based on a Cb tracking method that the author has proposed and then apply it in precipitation estimation using a look-up table algorithm.

2.3.1. Cloud Parameters

To describe the characteristics of Cb both from the pixel and cloud patch levels, 31 parameters were extracted from 3 FY-2C imagery channels (IR_1, 10.3–11.3 μm; IR_2, 11.5–12.5 μm and WV 6.3–7.6 μm), as shown in Table 1. In terms of the pixel features, 3 types of cloud features were extracted: coldness features, time series features and situation features. As for the cloud patch features, 4 types of cloud features were derived based on Cb tracking: coldness features, geometric features, cloud texture/structure and cloud dynamic features.

Those cloud features can be described as follows:

(1) The top brightness temperature of the Cb pixel (TB): The TB of the infrared channels.

(2) The gradient of pixel TB (GT): GT is the gradient of the TB for three infrared channels with a window size of 3 × 3 pixels, centered on pixel i (x,y):

$$GT_{(x,y)} = [(TB_{(x+1,y)} + TB_{(x-1,y)})^2 + (TB_{(x,y+1)} - TB_{(x,y-1)})^2]^{1/2} \quad (1)$$

(3) The difference of pixel TB over split-window channels (DT): DT is the difference in TB over split-window channels (IR Channels a and b):

$$DT_{ab(x,y)} = TB_{a(x,y)} - TB_{b(x,y)} \quad (2)$$

(4) The change ratio of pixel TB (CT):

$$CT_{(x,y)} = \frac{1}{\Delta t} \frac{TB_{t\ 1(x,y)} - TB_{t(x,y)}}{TB_{t\ 1(x,y)}} \quad (3)$$

In this study, Δt is typically 1 hour.

(5) The deviation of the convective cloud center (DCC): DCC is the distance of pixel i (x, y) to the Cb patch center (x_0, y_0):

$$DCC_{(i,j)} = ((x_0 - x)^2 + (y_0 - y)^2)^{1/2} \quad (4)$$

The center of the Cb patch can be the geometric center (X_{Geo},Y_{Geo}) or the gravitational center (X_{Gra},Y_{Gra}).

(6) The minimum TB of a cloud patch ($T_{min}P$):

$$T_{\min}P = \min_{(x,y)\in A}\{TB(x,y)\} \tag{5}$$

(7) The mean TB of a cloud patch ($T_{mean}P$):

$$T_{mean}P = \sum_{(x,y)\in A}\{TB(x,y)\}/N \tag{6}$$

where N is the number of pixels in a Cb patch.

(8) The difference in TB over split windows for a Cb patch (DSWT):

$$DSWT = T_{mean}P_{IR1} - T_{mean}P_{IR2} \tag{7}$$

(9) The difference in TB over IR and WV windows for a Cb patch (DIWT):

$$DIWT = T_{mean}P_{IR1} - T_{mean}P_{WV} \tag{8}$$

(10) The cloud patch area (Area):

$$Area = N \times pixel\ resolution \tag{9}$$

(11) The cloud patch perimeter (PERI):

$$PERI = N_{bound} \times pixel\ resolution \tag{10}$$

where N_{bound} is the number of pixels on the boundary of a Cb patch.

(12) The shape index of geometric momentum (SIGM): SIGM is defined as the ratio of the geometric momentum of a cloud patch, I, to that of a round patch with the same size (I_0):

$$SIGM = I / I_0 \tag{11}$$

where:

$$I = \sum_{i=1}^{N}[(x - x_{Geo})^2 + (y - y_{Geo})^2] \tag{12}$$

and (x, y) is the coordinate of pixel i, (x_{Geo}, y_{Geo}) is the geometric center of the cloud patch and I_0 is the geometric momentum of a round patch with the same area.

(13) The shape index of the perimeter (SIP): SIP is defined as the ratio of the perimeter ($PERI$) of a cloud patch to that of a round patch with the same area ($PERI_0$):

$$SIP = PERI / PERI_0 \tag{13}$$

(14) The eccentricity (ECCT): ECCT is defined as:

$$ECCT = c / a \tag{14}$$

where c is the distance between the focus and the center of the ellipse and a is the length of the long axis.

(15) The boundary steepness (BS): BS measures how steeply the temperature increases along the boundary of a cloud patch:

$$BS = \frac{\sum_{i=1}^{N_{bond}} \mu_b(i)}{N} \tag{15}$$

where $\mu_b(i)$ is the distance from pixel i on the cloud patch boundary to the corresponding position on the warmer cloud patch boundary.

(16) The standard deviation of the TB of a cloud patch (STD):

$$STD = \left\{ \sum_{(x,y)\in A} [TB(x,y) - T_{mean}PD]^2 / (N-1) \right\}^{1/2} \quad (16)$$

(17) The TB gradient of cloud patch (TGOP): TGOP is defined as the average temperature gradient from the shooting top ($T_{min}P$) to every pixel on the Cb boundary:

$$TGOP = \sum_{i=1}^{N} \frac{1}{\mu(i)} / N \quad (17)$$

where $\mu(i)$ is the distance from pixel i on the boundary to the shooting top ($T_{min}P$).

(18) The life stage of a cloud patch (LF) [23]: the lifecycle of a Cb patch is divided into 8 stages (LF1: the birth of a new cloud patch; LF2: the development of a single cloud patch; LF3: the dissipation of a single cloud patch; LF4: the merger of cloud cells; LF5: the dissipation of a single cloud patch into several cloud patches (the complex dissipation of a single cloud patch); LF6: the development of cloud cells; LF7: the dissipation of cloud cells; LF8: uncertain cloud patch)

(19) The horizontal moving speed of a Cb patch (HMSP) [23]: HMSP is the displacement of the cloud patch centers between two successive images divided by the time interval between the images.

(20) The horizontal moving direction of a cloud patch (HMDP) [23]: HMDP is a measure of the displacement of the cloud patch center in two successive images.

(21) The cloud growth rate (CGR) [23]*:* CGR is the ratio of the area of a cloud patch to its area in a previous image.

(22) The vertical moving characteristic of a Cb patch (VMCP) [23]: VMCP is represented by the ratio of the average TB of a Cb patch to the average TB it showed in a previous image, in that cloud top TB can reflect the height of a convective cloud, as well.

2.3.2. Parameter Extraction

The parameter extraction was based on a tracking system that consists of three steps: the identification of Cb pixels using an artificial neural network (ANN) classifier; the detection of homogeneous Cb patches with a seeded region growing (SRG) algorithm; and the establishment of a relationship between current and previous Cb patches using a cross-correlation-based approach.

(1) Cloud classification. This study used an artificial neural network (ANN) classifier to extract Cb clouds from multi-channel data as a pre-processing procedure to identify homogeneous consistent Cb patches and to reduce the uncertainty stemming from the TB thresholds. The ANN classifier is a biologically-inspired computer program designed to simulate the way in which the human brain processes information. It is a promising modeling technique, especially for data sets having non-linear relationships, which are frequently encountered in cloud classification processes. In this study, The ANN classifier divided cloud/surface into seven categories: sea, stratocumulus and altocumulus, mixed cloud, altostratus and nimbostratus, cirrostratus, thick cirrus and cumulonimbus, using 2,864 cloud samples manually collected by two experienced meteorologists (Dr. Chun-xiang Shi and Professor Xu-kang Xiang)

in June, July and August in 2007 from three FY-2C channel (IR_1, 10.3–11.3 μm; IR_2, 11.5–12.5 μm and WV 6.3–7.6 μm) imagery. Additionally, 15 features were chosen with numerous tests: 3 gray features (G_1,G_2, G_3), 3 spectral features (TB_1,TB_2, TB_3) and 9 assemblage features (G_1-G_2, G_1-G_3, G_2-G_3, TB_1-TB2, TB_1-TB_3, $TB2-TB3$, $(G_1-G_2)/G1$, $(G_1-G_3)/G1$, $(G_2-G_3)/G_2$). The ANN classifier was composed of 2 hidden layers, and the neurons of the first and the second layer are 9 and 4, respectively. The learning step and the learning momentums were sets as 0.1 and 0.7, and hyperbolic tangent function was used as the transfer function. More detail about the cloud classification procedure can be seen in Liu *et al.* [22].

Table 1. Cloud characteristics derived from geostationary imageries. Cb, cumulonimbus; TB, top brightness; IR, infrared; WV, water vapour.

Type	Features*	No.	Parameters**
Pixel features	Coldness features	1	Top brightness temperature of the Cb pixel (TB):TB_1, TB_2, TB_3
		2	Gradient of the pixel TB (GT): GT_1, GT_2, GT_3
		3	Difference of the pixel TB for IR channels (DT): DT_{21}, DT_{31}, DT_{32},
	Time evolution features	4	Changing ratio of the pixel TB (CT): CT_1, CT_2, CT_3
	Situation features	5	Deviation to the convective cloud center (DCC ***): DCC_1, DCC_2
Cloud patch features	Coldness features	6	Minimum TB of cloud patch ($T_{min}P$)
		7	Mean TB of cloud patch ($T_{mean}P$)
		8	Difference of Cb patch TB for the split window (DSWT)
		9	Difference of Cb patch TB for IR and WV channel (DIWT)
	Geometric features	10	Cloud patch area (Area)
		11	Perimeter (PERI)
		12	Shape index of the geometric inertia momentum (SIGM)
		13	Shape index of the perimeter (SIP)
		14	Eccentricity (ECCT)
	Texture features	15	Boundary steepness (BS)
		16	Standard deviations of the cloud patch (STD)
		17	TB gradient of cloud patch(TGOP)
	Dynamical features	18	Life stage factor of the cloud patch (LF)
		19	Horizontal moving speed of a Cb patch (HMSP)
		20	Horizontal moving direction of cloud patch (HMDP)
		21	Cloud growth rate (CGR)
		22	Vertical moving characteristic of cloud patch (VMCP)

Note: * Coldness features indicate the property of the cloud top brightness temperature. Time evolution features are the change of the cloud property in successive satellite pictures. Situation features demonstrate the site of the target pixel. Geometric features show the geometric shape of a cloud patch. Texture features are the surface characteristic of the cloud top of a Cb patch. Dynamical features indicate the development of a cloud patch on the spatial and temporal scale. ** The subscript of a parameter denotes the remote sensing data used in the calculation. For example, TB_1 means TB of channel IR1 (10.3–11.3 μm), TB_2 and TB_2 are the same as TB_1, but for channel IR_2 (11.5–12.5 μm) and channel WV (6.3–7.6 μm). DT_{21} means the difference of TB for IR_2 and IR_1. *** DCC_1 is the deviation to the geometric center, and DCC_2 is the deviation to the gravity center.

The accurate rates were shown in a confusion matrix using 274 testing samples (Table 2). It can be seen that the cloud classifier can differentiate cumulonimbus well, and the possibility of misjudging other types of clouds as Cb was low, with an error rate below 6%.

(2) Cloud segmentation. The seeded region growing (SRG) segmentation algorithm was used to extract cloud boundaries and segment Cb patches based on the result of ANN cloud classification.

(3) Cb tracking. This paper employed a cross-correlation-based approach, the most common technique of cloud tracking to track Cb patches. Then, the different stages of development of Cb were detected and classified into 8 types, as shown in (18) of Section 2.3.1.

Table 2. Confusion matrix of the cloud classification using the artificial neural network (ANN) classifier [22].

Classes	Sea*	Land	Low-Level Clouds	Midlevel Clouds	Thin Cirrus	Thick Cirrus	Multi-Layer Clouds	Cumulonimbus
Sea **	1	0	0	0	0	0	0	**0**
Land	0	0.97	0	0.01	0.01	0.01	0	**0**
Low-level clouds	0.04	0.05	087	0.02	0.02	0	0	**0**
Midlevel clouds	0.01	0	0.02	0.92	0.05	0	0	**0**
Thin cirrus	0.01	0.01	0.02	0.01	0.93	0.02	0	**0**
Thick cirrus	0	0	0	0.01	0.02	0.92	0.05	**0**
Multi-layer clouds	0	0	0	0.03	0	0.01	0.9	**0.06**
Cumulonimbus	0	0	0	0	0	0.01	0.01	**0.98**

Note: * observed by experience; ** classified by ANN.

2.3.3. The Analysis of the Relationship

A thorough analysis of the relationship between precipitation (rain rate and probability) and Cb cloud properties at both the pixel and cloud patch scales is performed.

Table 3. The number of Cb samples by matching gauge rainfall observations to satellite-derived cloud parameters.

Year	Month	Number of Cb Samples on Pixel Scale			Number of Cb Samples on Cloud Patch Scale		
		Cb	Cb with Precipitation	Ratio of Precipitation (%)	Cb	Cb with Precipitation	Ratio of Precipitation (%)
2007	5	209	61	29.19	48	15	31.25
	6	2034	691	33.97	905	443	48.95
	7	10,914	4225	38.71	1880	718	38.19
	8	9663	3339	34.55	1495	680	45.48
	9	3744	919	24.55	675	237	35.11
	10	1869	397	21.24	367	182	49.59
2008	7	9102	3632	39.90	1423	684	48.07
Total		37,535	13,264	35.34*	6793	2959	43.56*

Note: * average ratio of seven months.

(1) Pixel scale. The analysis of the relationship between precipitation and cloud pixel properties was carried out based on matching gauge rainfall observations to satellite-derived cloud parameters. The shortest distance principal was applied, in which a pixel whose distance from the center to the target gauge was the nearest was treated as the matched pixel. In this study, 37,535 Cb samples were collected in the 7 months of 2007 and 2008, as shown in Table 3, and 13,264 of them produced precipitation. Those sampled during June and October 2007, were used to analyze the precipitation relationship on the pixel scale.

Considering the limitations of the correlation coefficient in describing the non-linear relationship, this study adopted the interval variable method as the interval rainfall probability (IRP) method used by Xu *et al.* [1]. The range of a cloud features is divided into equal-length intervals, and the rain rate and probability are then computed on each of these intervals.

(2) Cloud patch scale. *T*he analysis of the precipitation relationship on the cloud patch scale was the same as that on pixel scale, but for the matching method of samples. In this study, matching to the satellite-derived cloud property on the cloud patch scale was made based on the spatial resampling of the area rainfall distribution from gauge observations with the kriging interpolation method as pre-processing. Thus, a total of 6793 cloud patch samples were collected, and 2959 of them produced precipitation, as shown in Table 3.

2.3.4. The Application of the Relationship

This paper attempts to estimate precipitation with a lookup table method, which is a simple, non-linear method, based on the relationship between precipitation and cloud properties identified previously.

Table 4. The correlation coefficient (Corr) of the rain rate and cloud parameters.

No.	Parameters	Corr	Chosen ※	No.	Parameters	Corr	Chosen	No.	Parameters	Corr	Chosen
1	TB_1	−0.352 **	1	12	CT_3	−0.128	0	23	ECCT	−0.029	0
2	TB_2	−0.343 **	0	13	DCC_1	−0.013	0	24	BS	−0.199	0
3	TB3	−0.306 *	0	14	DCC_2	−0.016	0	25	STD	0.086	0
4	GT_1	−0.172	0	15	$T_{min}P$	−0.044	0	26	TGOP	−0.016	0
5	GT_2	0.081	0	16	$T_{mean}P$	−0.032	0	27	LF	0.269 *	1
6	GT_3	−0.309 *	1	17	DSWT	0.161	0	28	HMSP	0.089	0
7	DT_{21}	−0.081	0	18	DIWT	0.079	0	29	HMDP	−0.215	0
8	DT_{31}	−0.306 *	1	19	Area	0.330 *	1	30	CGR	0.288*	1
9	DT_{32}	−0.302	0	20	PERI	0.268 *	1	31	VMCP	−0.194	0
10	CT_1	0.018	0	21	SIGM	−0.243	0				
11	CT_2	−0.332 *	1	22	SIP	−0.033	0				

Note: ※ The parameters are chosen to construct the lookup table. * Correlation is significant at the 0.05 level; ** Correlation is significant at the 0.01 level.

(1) Model inputs. To reduce the dimensionality of the input data, the threshold principle of correlation coefficients was applied. A cloud pixel parameter, whose correlation coefficient with a rain rate over 0.3 was thought to be a relatively important factor, was selected as an input. Thus, 7 pixel parameters (TB_1, TB_2,

TB_3, GT_3, DT_{31}, DT_{32} and CT_2) and 2 cloud patch parameters (Area, PERI) were chosen in this study. Considering the similarity of some pixel cloud parameters, they can be reduced to 4 (TB_1, GT_3, DT_{31}, CT_2).

In terms of the cloud patch dynamic character, some parameters, such as CGR and LF, were added to the input lists because of their close relationship to rainfall according to the above analysis, despite their low correlation coefficients (<0.3), which stems from the typical non-linear relationship between the cloud parameters and rain. Thus, a total of 8 parameters (4 pixel parameters: TB_1, GT_3, DT_{31}, CT_2; 4 cloud patch parameters: Area, PERI, LF, CGR) were chosen (Table 4). TB_1, GT_3, and DT_{31} indicate the influence of coldness features on precipitation on pixel scale, and CT_2 shows the variation of Cb cloud property. Area, and PERI demonstrated the influence of geometric shape on precipitation on cloud patch scale, while LF, and CGR indicate the development.

(2) Configuration. Considering the limited samples, it is hard to establish a traditional look-up table. This study used a simplified one, which contained four steps: (a) establish a look-up table of the rain rate and rain probability for each cloud parameter based on the curve of precipitation and cloud properties used in the previous analysis; (b) estimate the rain rate and rain probability for each cloud parameter with the corresponding look-up tables; (c) calculate the rain probability (RP_1, RP_2… RP_8) and rain rate (RR_1, RR_2…RR_8) for 8 cloud parameters based on the look-up tables obtained in Step b; (d) exclude rare rain events by setting the rain probability as 0 if the sum of those 8 rain probabilities ($RP\_sum = RP_1 + RP_2 + \ldots + RP_8$) obtained in Step c is less than 80%, with the assumption that no rain event takes place if the average rain probability is not more than 10%; (e) normalize the rain probability of individual cloud parameters by dividing them with the sum of the 8 rain probabilities (RP_1/RP_sum, RP_2/RP_sum…RP_8/RP_sum); and (f) estimate the rain rate by using the normalized rain probability as the weight to combine the rain rate of individual cloud parameters obtained in Step c ($RR_1 \times RP_1/RP\_sum + RR_2 \times RP_2/RP\_sum + \ldots + RP_8 \times RP_8/RP\_sum$).

(3) Training and testing. To determine the relationship between the input cloud properties and output precipitation, this study developed the precipitation estimation model using 6 months of data in 2007 (6.2007–10.2007) and tested it using 2 months of data (5.2007 and 7.2008). Two-thirds (18,866 samples) of the development data were randomly chosen to train the model, while the rest of the data (9,408 samples) were used for cross-validation.

(4) Evaluation indices. Several criteria were selected to evaluate the performance of the precipitation estimation, such as the correlation coefficient (Corr), the root-mean-square error (RMSE), the probability of detection (POD), the false alarm ratio (FAR) and the critical success index (CSI). The former two were used to test the accuracy of the estimation; the latter three were used to evaluate the performance of the rain/no-rain detection. Definitions of these criteria are listed in the report of the third Algorithm Intercomparison Project of the Global Precipitation Climatology Project [24].

3. Results

The relationship between precipitation and Cb features was determined at the pixel and cloud patch scales. Then, a case of its application in the rainfall estimation was given.

3.1. Relationship between Precipitation and Pixel Features

Figure 1 shows the relationship between precipitation and three pixel features of the Cb cloud, namely coldness features, time evolution features and situation features. The results show that the rain probability is randomly higher than 50%. In addition, the rain probability has a variation similar to that of the rain rate in that there is not a linear relationship between cloud features and Cb precipitation. This result illustrates the difficulty of estimating Cb precipitation and the necessity of building a non-linear model.

(1) Coldness Features

This study used the two parameters of cloud coldness features to illustrate the developmental characteristics of the Cb clouds: the height of the cloud top by the brightness temperature (TB) and the convection strength by the gradient of the TB (GT). Normally, clouds in the development stage correspond to a high cloud top and strong convection, which can be indicated by less TB and more GT values, and *vice versa* for clouds in the stable stage.

Figure 1a–c is the precipitation characteristic of the TB for three infrared channels (IR_1, IR_2 and WV). The results show the following: (a) Precipitation with a high rate and probability always occurs with 198–218 K of TB_1, 200–222 K of TB_2 and 205–222 K of TB_3. The variation in the probability is less dramatic compared to that of the rain rate. (b) The rain rate and probability first increase then decrease rapidly with increasing TB_1, which varies similarly to TB_2 and TB_3 and is consistent with previous studies [4,25]. This indicates that heavy rainfall is always associated with strong convection. However, the strongest convection is not necessary to produce the greatest rainfall.

Figure 1. The relationship between cloud pixel characteristics and precipitation in the Huaihe River Basin (HRB). (**a**) Precipitation characteristic of top brightness temperature (TB) for infrared channel 1 (IR_1) (10.3–11.3 μm); (**b**) and (**c**) are the same as (**a**) but for channel IR_2 (11.5–12.5 μm) and channel WV (6.3–7.6 μm); (**d**)–(**f**): the same as (**a**)–(**c**) but for the gradient of pixel TB (GT) for IR_1, IR_2 and WV channels (GT_1, GT_2, GT_3), respectively; (**g**)–(**i**): the same as (**a**)–(**c**) but for the difference of pixel TB (DT) for three IR channels (DT_{21}, DT_{31}, DT_{32}), respectively. DT_{21} is the difference of TB of IR_2 and IR_1. DT_{31} is the difference of WV and IR_1, and DT_{32} is the difference of WV and IR_2; (**j**)–(**l**): the same as (**a**)–(**c**) but for the changing ratio of pixel TB (CT) for three IR channels (CT_1, CT_2, CT_3), respectively; (**m**)–(**n**): the same as (**a**)–(**c**) but for deviation to the convective cloud center (DCC). DCC_1 is the deviation to the geometric center, and DCC_2 is the deviation to the gravity center.

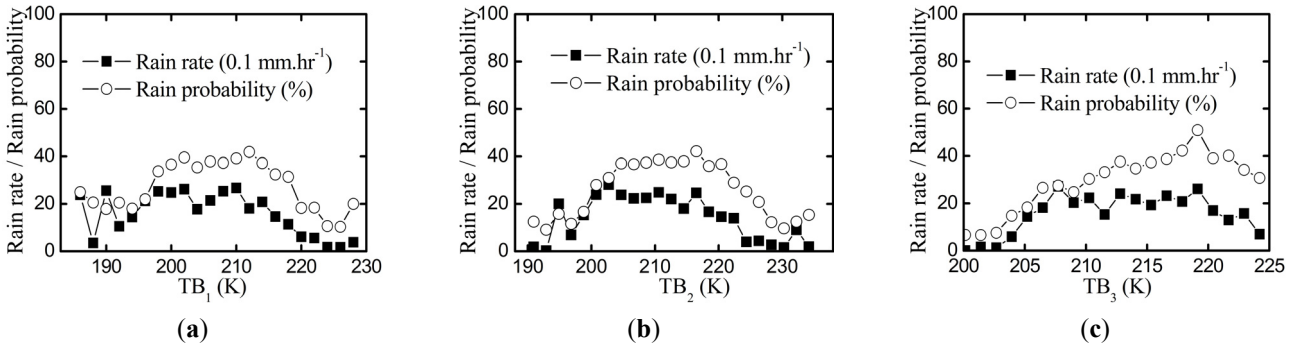

Figure 1. *Cont.*

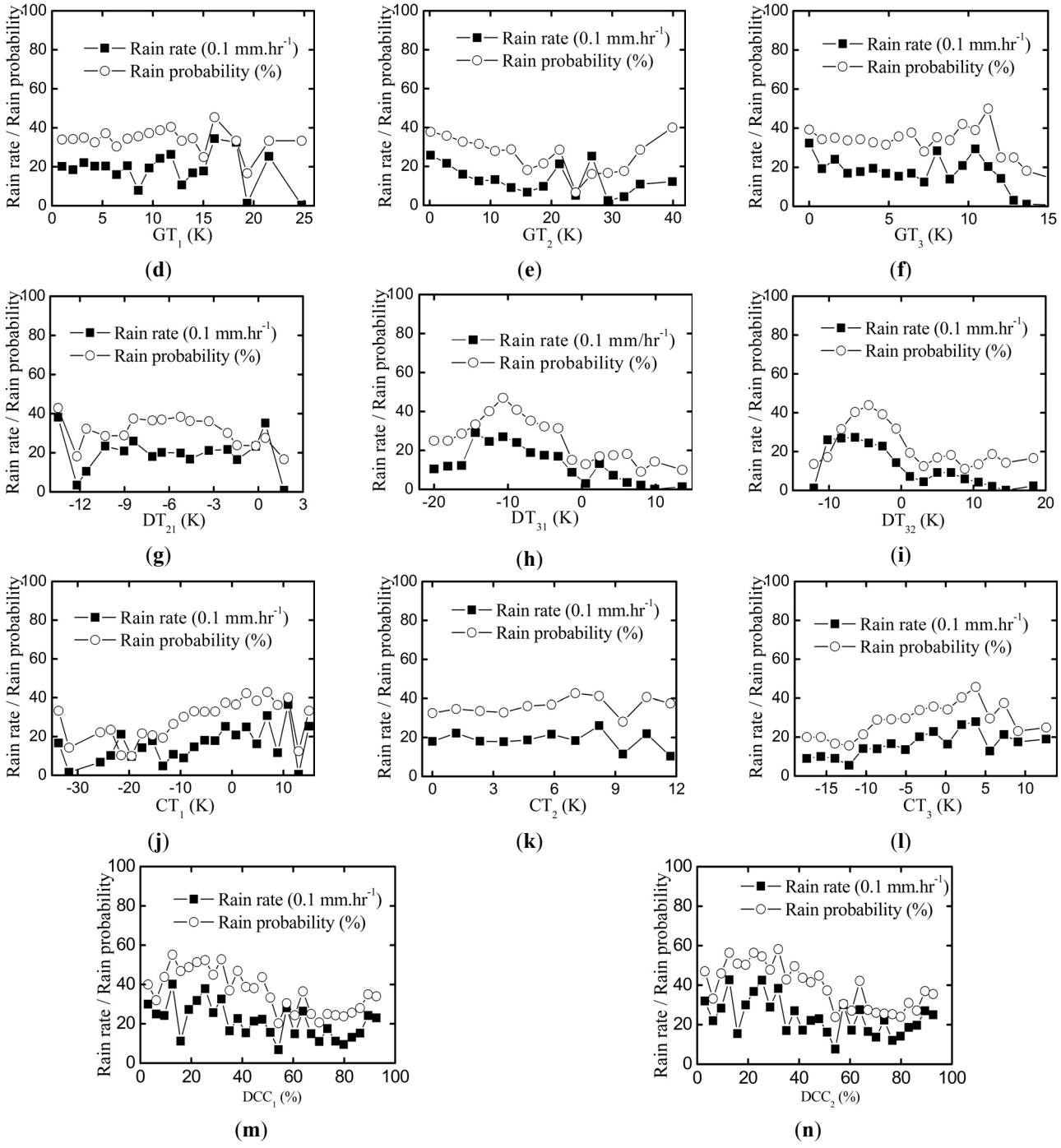

The GT of three infrared channels with a window size of 3 × 3 can be observed in Figure 1d–f. The result shows the following: (a) Heavy rainfall occurs during the initial stage of convection with the greatest value for GT_2 and a stable stage with the smallest absolute value for GT_2 (GT_2 = 0). (b) Compared to GT_1 and GT_3, GT_2 is more suitable for characterizing the link between rainfall and cloud GT features. On the one hand, the range of GT_2 is broader, between 0 K and 40 K, while the range of GT_2 is 0–25 K and GT_3 is 0–20 K, which are narrower. In contrast, the change in the rain probability is more sensitive to GT_2, varying between 5 K and 40%, whereas GT_1 and GT_3 are 20%–40%.

(2) Differences of the IR Channels

The difference of the TB (DT) can indicate the height and developmental characteristics of convective clouds and are usually used to discriminate Cb and other underlying clouds. The DTs of the three channels (DT_{21}, DT_{31} and DT_{32}) are shown in Figure 1g–i, indicating that: (a) Precipitation takes place with −12–2 K of DT_{21}, −20–15 K of DT_{31} and −12–18 K of DT_{32}; strong precipitation always occurs when DT_{31} and $DT_{32} < 0$, and both the rain rate and probability are low when DT_{31} and $DT_{32} > 0$. (b) Precipitation first increases and then decreases with increasing $DT_{31}$and DT_{32}, which is similar to the variation of TB. (c) The rain rate and probability are more sensitive to DT_{31} and DT_{32} than DT_{21} in that the curve of DT_{21} is flatter. Therefore, the DT_{31} and DT_{32} are more applicable to precipitation estimation.

(3) Time Evolution Features

This study used the changing ratio of pixel TB (CT) to illustrate the cloud development on the vertical height for strong conviction corresponds to the cold cloud top. Figure 1j–l is the CT curve for the three channels (CT_1, CT_2 and CT_3). It can be observed that: (a) Precipitation takes place with −35–20 K of CT_1, 0–12 K of CT_2 and −18–13 K of CT_3. Heavy rain predominantly takes place when the clouds are in the stages of development with CT > 0. Both the rain rate and probability increase first and then decrease with increasing CT, which is consistent with the previous TB and DT study. (c) When CT < 0, the rain rate and probability are never high during the cloud dissipation process and decrease with increasing CT. However, some strong rain events still exist, such as the rainfall event near −32 K of CT_1 and −17 K of CT_3, which may be associated with the occurrence of overshooting tops and the rapid horizontal movement of Cb cloud tops.

(4) The Deviation of the Cloud Center (DCC)

Figure 1m–n includes the Cb precipitation characteristics related to the deviation of the convective cloud center, such as the geometric center (DCC_1) and gravity center (DCC_2). The results show that deviations in the cloud gravity center and geometric center have almost the same influence on precipitation and that heavy precipitation may occur not only in the convective center with DCC = 0, but also on the front of convective clouds with high DCC.

3.2. Relationship between Precipitation and the Cloud Patch Character

The distributions of the rain rate and the probability for four types of cloud patch features (geometric features, coldness features, texture/structure features and dynamic features) are shown in Figure 2.

(1) Geometric Features

As shown in Figure 2a–e, this study used five parameters, Area, PERI (perimeter), SIGM (shape index of the geometric inertia momentum), SIP (shape index of the perimeter) and ECCT (eccentricity), to describe the geometric features of Cb clouds. The results shows that the curve of SIGM, SIP and ECCT varies complexly, and there are "double peaks and valleys" for the curve of Area and PERI. This indicates that precipitation takes place not only during the early stage of newly born Cb, but also during the rapidly

developing stage. Cb in the early stage are always small and nearly round, with low values for those geometric parameters compared to Cb in the developing and splitting stages, according to the observation.

Figure 2. The relationship between the cloud patch characteristics and precipitation in the HRB. (**a**) Distribution of rain variables and cloud patch area (Area); (**b**)–(**l**) are the same as (**a**) but for perimeter (PERI), shape index of the geometric inertia momentum (SIGM), shape index of the perimeter (SIP), eccentricity (ECCT), mean TB of cloud patch ($T_{mean}P$), minimum TB of cloud patch ($T_{min}P$), difference of Cb patch TB for the split window (DSWT), difference of Cb patch TB for IR and WV channel (DIWT), standard deviations of the cloud patch (STD), TB gradient of cloud patch(TGOP), and boundary steepness (BS), respectively.

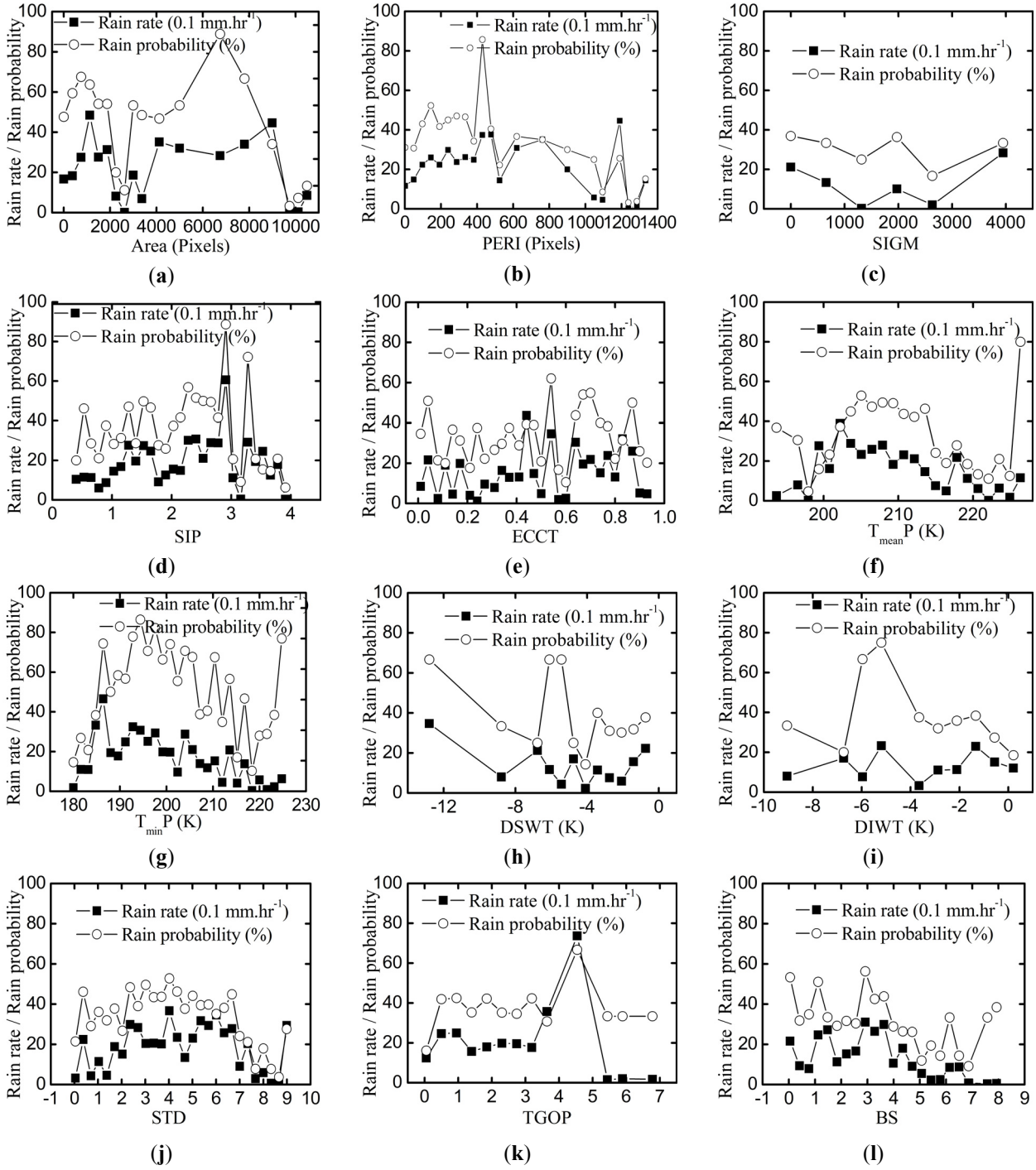

(2) Coldness Features

The relationship between precipitation and cloud coldness features is analyzed using four parameters: $T_{mean}P$ (the mean TB of the Cb patch), $T_{min}P$ (the minimum TB of the Cb patch), DSWT (the difference in the split window TB for the Cb patch) and DIWT (the difference in the IR and WV TB for the Cb patch) (Figure 2f–i). The results indicate that: (a) the curves for the coldness features of the cloud patch, such as $T_{mean}P$ and $T_{min}P$, are quite similar compared to those of the pixel, such as TB_1, TB_2 and TB_3; b) precipitation occurs when the DSWT and DIWT are negative and first decreases and then increases as the values of these variables fall below 0; c) strong precipitation occurs with $T_{mean}P$ 203–214 K, $T_{min}P$ 185–215 K, DSWT and DIWT −5–6 K; and (d) some rare strong precipitation events, with probabilities less than 20%, take place when the $T_{mean}P$ is less than 198 K or over 225 K, and DSWT/DIWT < −7 K.

(3) Texture/Structure Features

To illustrate the influence of the cloud texture/structure features on precipitation, this study analyzed three parameters: STD (the standard deviation of the cloud patch), TGOP (the top brightness temperature gradient of cloud patch) and BS (boundary steepness) (Figure 2j–l). The results show that: (a) Precipitation first increases and then declines with increasing STD. Precipitation reaches its highest value when the STD is four, and it reaches its lowest value when the STD is 8.6. This indicates that cloud patches with rough surfaces produce strong rain. However, cloud patches with the roughest surfaces do not necessarily produce the strongest rain, which is consistent with our previous study. (b) The rain rate does not change significantly when the TGOP increases from zero, but it began to increases rapidly when the TGOP is 3.2 and reaches its highest point when it is 4.5, with the probability increasing from 20% to 70%. (c) The precipitation varies complexly with the BS. On the whole, precipitation decreases with the increasing BS when the BS is less than seven, and the rain rate is almost zero when the BS is over six.

(4) Dynamic features

The precipitation curves for the five dynamics features (the life stage factor of the cloud patch (L), the horizontal moving speed of the cloud patch (HMSP), the horizontal moving direction of the cloud patch (HMDP), the cloud growth rate (CGR) and the vertical moving characteristic of the cloud patch (VMCP)) were shown by Liu *et al.* previous work [23]. Overall, precipitation varies significantly for Cb over the different life stages, and the rain intensity and the probability of single Cb patches are lower compared to those of complicated Cb patches, which involve some minor Cb patches. In addition, precipitation has no obvious relationship with cloud motion features, such as the horizontal moving speed of cloud patches (HMSP), the horizontal moving direction of cloud patches (HMDP) or the vertical moving characteristic of cloud patches (VMCP). There are “double peaks and valleys” for the curve of the cloud expansion rate (CGR). Heavy rainfall takes places with minor or great expansion of the convective cloud, while clouds in the dissipating stage or medium expansion produce less precipitation.

3.3. Application of the Rainfall Relationship in Precipitation Estimation

The estimation results of the hourly rainfall intensity during May and October of 2007 and July of 2008 are presented in Table 5 and Figure 3.

Table 5. The estimation result for the six-hour rain rate in 2007 and 2008. POD, probability of detection; FAR, false alarm ratio; CSI, critical success index.

Year	Month	Samples	Corr	Bias	RMSE	POD	FAR	CSI
Cross-validation	6.2007	678	0.47	−2.65	119.01	0.93	0.35	0.62
	7.2007	3638	0.70	−0.85	137.47	0.95	0.06	0.90
	8.2007	3221	0.69	−0.50	61.69	0.83	0.04	0.80
	9.2007	1248	0.43	0.80	47.03	0.36	0.10	0.35
	10.2007	623	0.26	0.80	20.31	0.33	0.15	0.31
	Average		0.62	−0.53	90.44	0.79	0.09	0.73
Testing	5.2007	204	0.41	−42.58	434.80	0.88	0.53	0.45
	7.2008	9102	0.51	−0.92	382.9	0.75	0.08	0.72
	Average		0.51	−1.83	384.04	0.75	0.09	0.71

Figure 3. Scatter plot of the estimated rain rate *vs.* the observed rain rate of the gauge. (**a**) Cross-validation results with data from June to October 2007; (**b**) testing results with data of May 2007 and July 2008.

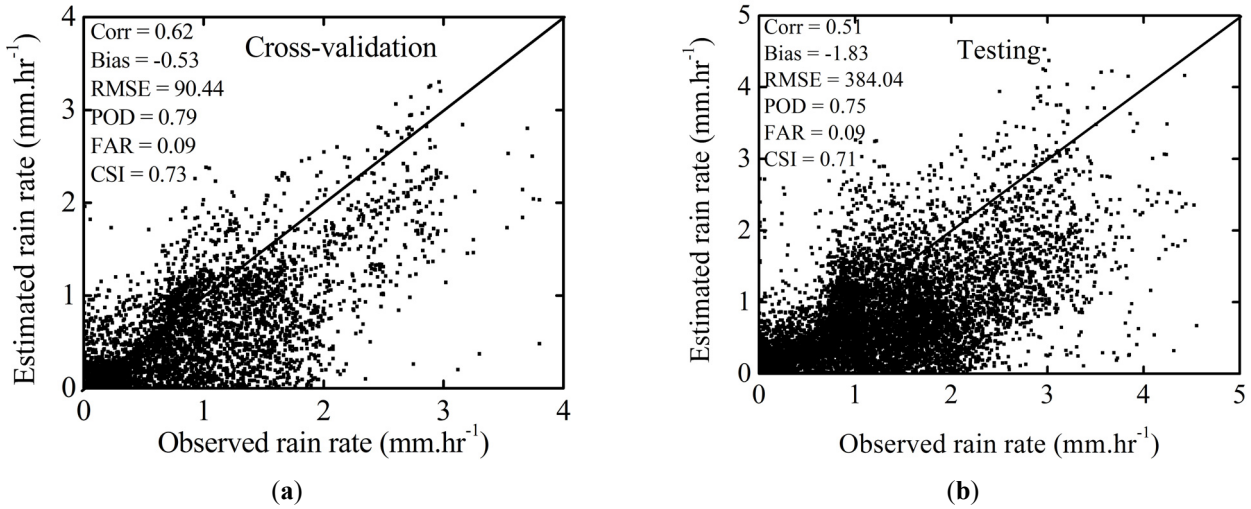

It can be observed that the proposed precipitation estimation method based on the relationship analyzed has an impressive performance, with an average Corr of 0.62, Bias of −0.53, an RMSE of 90.44, a POD of 0.79, a FAR of 0.09 and a CSI of 0.73 in the cross-validation period. The Corr of the rainfall estimation can reach 0.70 in some months. However, the performance in May is not so good. The reasons are that the HRB entered summer and the plum rain season from June, and it makes the relationship of precipitation and cloud characteristics that the modeling construction used before no longer applicable.

In the testing period, the POD, FAR and CSI were similar to those in cross-validation period. However, the Corr, Bias and RMSE were worse than the cross-validation period. This indicates that the

model can track the occupancy of precipitation events well, but the accuracy of the rain rate value was greatly influenced by the different precipitation cloud system. This also points to the necessity of collecting ample cloud samples to represent precipitation events.

In addition, the Corr in the testing period can reach 0.51 on average, whereas the correlation coefficients of some global rainfall estimation products are approximately 0.2−0.7, such as Climate Prediction Center (CPC) morphing technique (CMORPH) [26]; this also implied the further application of the method.

4. Conclusions

The work presented herein thoroughly analyzed the relationship between precipitation and the Cb cloud characteristics, both at the pixel and cloud patch scale, to provide deep insight into improving the accuracy of precipitation estimation. In terms of pixel features, three types of cloud features are derived: coldness features, time series features and situation features. As for the cloud patch features, four types of cloud features are illustrated based on Cb tracking: geometric features, coldness features, cloud texture/structure and cloud dynamic features. Furthermore, to apply the relationship of precipitation and the cloud properties identified, this study estimates the precipitation using a look-up table algorithm.

The results illustrate that in terms of pixel features, precipitation first increases and then declines as the increasing of coldness and the time series parameters, such as TB, GT, DT and CT. Moreover, heavy precipitation may occur not only in the convective center, but also in the forefront of convective clouds.

As for the cloud patch scale, precipitation activities are typically associated with cold clouds and rough cloud surfaces, which have low $T_{mean}P$, $T_{min}P$, DSWT and DIWT and high STD and TGOP, whereas the coldest and roughest cloud surfaces do not correspond to the heaviest rainfall. In addition, precipitation varies significantly over different life stages. Normally, heavy rain predominantly takes place during the early stages of newly born Cb and the developing stage, because of the "double peaks and valleys" phenomenon for geometric features (Area and PERI) and the dynamic feature (CGR). In addition, both the rain rate and the probability of a single Cb are lower compared to complicated Cb, which involve mergers and splits of some minor Cb patches. Motion features, such as the horizontal moving speed of cloud patches (HMSP), the horizontal moving direction of cloud patches (HMDP) and the vertical moving characteristic of cloud patches (VMCP) have no obvious impact on rain.

The correlation coefficients of the estimated rain rate and gauge rain can reach 0.62 in the cross-validation period and 0.51 in the testing period. The impressive result illustrates the feasibility of the further application of the relationship in rain estimation. In addition, these results also indicate that each cloud feature can provide a different perspective and helpful information in defining the characteristics of Cb. Therefore, employing a systematic analysis of these features is essential to providing an improved understanding of the Cb precipitation in the HRB and to thus improve the rainfall estimations of geostationary satellites.

Acknowledgments

This work was supported by the National Natural Science Foundation of China under grants 41301379 and 41231170 and the China Postdoctoral Science Foundation under grant 2013M541029. The authors would like to thank the National Weather Service Information Center of China for providing

FY2C and meteorological data. The authors greatly appreciated the careful and insightful suggestions and comments of reviewers that helped to improve the manuscript and data analysis.

Author Contributions

Conceived and designed the experiments: Yu Liu, Du-Gang Xi, Zhao-Liang Li, Chun-Xiang Shi. Performed the experiments of cloud classification, Cb segmentation: Yu Liu, Du-Gang Xi. Performed the experiments of Cb cloud tracking: Zhao-Liang Li, Chun-Xiang Shi. Analyzed the relationship between Cb cloud features and precipitation data: Yu Liu, Du-Gang Xi, Chun-Xiang Shi. Established the precipitation model: Yu Liu, Du-Gang Xi. Wrote the paper: Yu Liu, Zhao-Liang Li.

Conflicts of Interest

The authors declare on conflict of interest.

References

1. Xu, L.; Gao, X.; Sorooshian, S.; Arkin, P.A.; Iman, B. A microwave infrared threshold technique to improve the GOES precipitation index. *J. Appl. Meteorol.* **1999**, *38*, 569–579.
2. Kurino, T. A satellite infrared technique for estimating "deep/shallow" precipitation. *Adv. Space Res*. **1997**, *19*, 511–514.
3. Lu, N.M.; Wu, R.Z. Strong convective cloud characteristics derived from satellite cloud picture (In Chinese). *J. Appl. Meteorol. Sci.* **1997**, *8*, 270–275.
4. Arkin, P.A. The relationship between fractional coverage of high cloud and rainfall accumulations during GATE over the B-scale array. *Mon. Weather Rev.* **1979**, *107*, 1382–1387.
5. Hong, G.; Heygster, G.; Rodriguez, C.A.M. Effect of cirrus clouds on the diurnal cycle of tropical deep convective clouds. *J. Geophys. Res*. **2006**, doi:10.1029/2005JD006208.
6. Griffith, C.G.; Woodley, W.L.; Grube, P.G.; Martin, D.W; Stout, J.; Sikdar, D.N. Rain estimation from geosynchronous satellite imagery-visible and infrared studies. *Mon. Weather Rev.* **1978**, *106*, 1153–1171.
7. Negri, A.J.; Adler, R.F. Infrared and visible satellite rain estimation. Part II: A cloud definition approach. *J. Clim. Appl. Meteorol.* **1987**, *26*, 1565–1576.
8. Negri, A.J.; Adler, R.F.; Wetzel, P.J. Rain estimation from satellites: An examination of Griffith–Woodley technique. *J. Clim. Appl. Meteorol.* **1984**, *23*, 102–116.
9. Woodley, W.L.; Griffith, C.G.; Stroomatt, S.C. The inference of GATE convective rainfall from SMS-1 imagery. *J. Appl. Meteorol.* **1980**, *19*, 314–330.
10. Laurent, H.; D'Amato, N.; Lebel, T. How important is the contribution of the mesoscale convective complexes to the Sahelian rainfall? *Phys. Chem. Earth* **1998**, *23*, 629–633
11. Mathon, V.; Laurent, H.; Lebel, T. Mesoscale convective system rainfall in the Sahel. *J. Appl. Meteorol.* **2002**, *41*, 1081–1092.
12. Goyens, C.; Lauwaet, D.; Schroder, M.; Demuzere, M.; Van Lipziga, N.P.M. Tracking mesoscale convective systems in the Sahel: Relation between cloud parameters and precipitation. *Int. J. Climatol.* **2011**, *32*, 1921–1934

13. Vondou, D.A. Spatio-temporal variability of western central African convection from infrared observations. *Atmosphere* **2012**, *3*, 377–399.
14. Laing, A.G.; Carbone, R.E.; Levizzani, V. Cycles and propagation of deep convection over equatorial Africa. *Mon. Weather Rev.* **2011**, *139*, 2832–2853.
15. Zinner, T.; Mannstein, H.; Tafferner, A. Cb-TRAM: Tracking and monitoring severe convection from onset over rapid development to mature phase using multi-channel Meteosat-8 SEVIRI data. *Meteorol. Atmos. Phys.* **2008**, *101*, 191–210.
16. Machado, L.A.T.; Rossow, W.B.; Guedes, R.L., Walker, A.W. Life cycle variations of mesoscale convective systems over the Americas. *Mon. Weather Rev.* **1998**, *126*, 1630–1654.
17. Machado, L.A.T.; Laurent, H. The Convective system area expansion over Amazonia and its relationships with convective system life duration and high-level wind divergence. *Mon. Weather Rev.* **2004**, *132*, 714–725.
18. Arnaud, Y.; Desbois, M.; Maizi, J. Automatic tracking and characterization of African convective systems on meteosat pictures. *J. Appl. Meteorol.* **1992**, *31*, 443–453.
19. Zhao, S.X.; Zhang, L.S.; Sun, J.H. Study of heavy rainfall and related mesoscale systems causing severe flood in Huaihe rixdver basin during the summer of 2007 (in Chinese). *Clim. Environ. Res.* **2007**, *12*, 713–727.
20. Zhou, Y.S.; Li, B. Structural analyses of vortex causing torrential rain over the Changjiang-Huaihe River Basin during 8 and 9 July 2003 (in Chinese). *Chin. J. Atmos. Sci.* **2010**, *34*, 629–639.
21. Jiao, M.Y.; Yao, X.X.; Zhou, B.; Yang, K.M. *Analysis and Research of Heavy Rainfalls Causing Flood in Huaihe River in 2003* (in Chinese); Meteorological Press: Beijing, China, 2004; p. 215.
22. Liu, Y.; Xia, J.; Hong, Y.; Shi, C.X. An improved cloud classification algorithm for China's FY-2C multi-channel images using artificial neural network. *Sensors* **2009**, *9*, 5558–5579.
23. Liu, Y.; Li, Z.L.; Shi, C.X.; Tang, B.H.; Wu, H.; Liu, Q.C. Relation between cumulonimbus(Cb) precipitation and cloud dynamical features over Huaihe river Basin of China based on FY-2C image. In Proceedings of IEEE International Geoscience and Remote Sensing Symposium, Melbourne, VIC, Australia, 21–26 July 2013; pp. 554–557
24. Ebert, E.E. *Results of the 3rd Algorithm Intercomparison Project* (*AIP-3*) *of the Global Precipitation Climatology Project* (*GPCP*); Bureau of Meteorology Research Centre: Melbourne, VIC, Australia, 1996.
25. King, P.W.S.; Hogg, W.D.; Arkin, P.A. The role of visible data in improving satellite rain-rate estimates. *J. Appl. Meteorol.* **1995**, *34*, 1608–1621.
26. Xie, P.P.; Chen, M.Y.; Yang, S.; Yatagai, A.; Hayasaka, T.; Fukushima, Y.; Liu, C.M. A gauge-based analysis of daily precipitation over East Asia. *J. Hydrol.* **2007**, *8*, 607–626.